Design of Highly Oleophobic Cellulose Surfaces from Structured Silicon Templates

Christian Aulin,*,†,‡ Sang Ho Yun,§ Lars Wågberg,‡ and Tom Lindström||

BIM Kemi AB, Box 3102, SE-443 03 Stenkullen, Sweden, Department of Fibre and Polymer Technology, School of Chemical Science and Engineering, and Department of Microelectronics and Applied Physics, School of Information and Communication Technology, The Royal Institute of Technology, SE-100 44 Stockholm, Sweden, and STFI-Packforsk AB, Box 5604, SE-114 86 Stockholm, Sweden

ABSTRACT Structured silicon surfaces, possessing hierarchical porous characteristics consisting of micrometer-sized cavities superimposed upon a network of nanometer-sized pillars or wires, have been fabricated by a plasma-etching process. These surfaces have superoleophobic properties, after being coated with fluorinated organic trichlorosilanes, on intrinsically oleophilic surfaces. By comparison with flat silicon surfaces, which are oleophilic, it has been demonstrated that a combination of low surface energy and the structured features of the plasma-etched surface is essential to prevent oil from penetrating the surface cavities and thus induce the observed macroscopic superoleophobic phenomena with very low contact-angle hysteresis and low roll-off angles. The structured silicon surfaces were coated with cellulose nanocrystals using the polyelectrolyte multilayer technique. The cellulose surfaces prepared in this way were then coated with a monolayer of fluorinated trichlorosilanes. These porous cellulose films displayed highly nonwetting properties against a number of liquids with low surface tension, including alkanes such as hexadecane and decane. The wettability and chemical composition of the cellulose/silicon surfaces were characterized with contact-angle goniometry and X-ray photoelectron spectroscopy, respectively. The nano/microtexture features of the cellulose/silicon surfaces were also studied with field-emission scanning electron microscopy. The highly oleophobic structured cellulose surfaces are very interesting model surfaces for the development of biomimetic self-cleaning surfaces in a vast array of products, including green constructions, packaging materials, protection against environmental fouling, sports, and outdoor clothing, and microfluidic systems.

KEYWORDS: superoleophobic • cellulose • surface roughness • low surface energy • nanocrystals • polyelectrolyte multilayer • XPS • SEM • oil repellent • coating

INTRODUCTION

Surfaces with water contact angles greater than 150° and low roll-off angles are typically referred to as superhydrophobic or super-water-repellent. Such surfaces are observed in nature on plant leaves (1) and insects (2−5). Water on these surfaces forms beads and drips off rapidly while washing away contaminations. This phenomenon renders materials with superhydrophobic surfaces self-cleaning. The observed self-cleaning property of natural superhydrophobic surfaces has stimulated extensive research into the fabrication of artificial superhydrophobic surfaces as well as the study of the fundamental mechanisms underlying the behavior of a liquid on such surfaces (2, 6−14). Studies regarding superoleophobic surfaces, i.e., structured surfaces that resist wetting by liquids with a much lower surface tension than water, such as hexadecane and decane, are, nevertheless, very rare (15−19). Potential applications are numerous and include self-cleaning products, green constructions, packaging materials, protection against environmental fouling, sports, and outdoor clothing, and microfluidic systems (17, 20, 21).

The wettability of a solid surface is determined by two factors, viz., the chemical composition and the topographic structure (17, 22−24). Modifying the surface with chemical groups that can create a low surface free energy can effectively increase the contact angle of oil on a solid surface. So far, the trifluoromethyl group (CF_3)-terminated surface has been reported to possess the lowest surface free energy (25, 26) and thus the highest water ($\theta_{water} \approx 100°$) and oil ($\theta_{hexadecane} \approx 91°$) contact angles on a flat surface. To increase the contact angles further, the surfaces need to be roughened. Typically, if the contact angle on a flat surface (θ_{flat}, also referred to as the intrinsic contact angle of the surface) is greater than 90°, then roughening the surface will result in an apparent contact angle (θ_{rough}) that is greater than θ_{flat}, whereas if θ_{flat} is less than 90°, a roughening of the surface will result in θ_{rough} that is less than θ_{flat}. Artificial superhydrophobic surfaces have therefore been prepared either by creating a tailored topography on a hydrophobic material or by chemically treating a rough surface to induce a low surface free energy of the material (12, 13, 20). Either approach requires a θ_{flat} greater than 90° in order to increase the hydrophobicity by tuning the surface topography.

Two distinct models, developed independently by Wenzel (27) and by Cassie and Baxter (28) (henceforth, referred to

* E-mail: caulin@polymer.kth.se.

Received for review June 05, 2009 and accepted October 12, 2009

† BIM Kemi AB.

‡ Department of Fibre and Polymer Technology, School of Chemical Science and Engineering, The Royal Institute of Technology.

§ Department of Microelectronics and Applied Physics, School of Information and Communication Technology, The Royal Institute of Technology.

|| STFI-Packforsk AB.

DOI: 10.1021/am900394y

as the Cassie model), are commonly used to explain the effect of roughness on the apparent contact angle of a liquid drop on a solid surface (22). The Wenzel model recognizes that the surface roughness increases the available surface area of the solid and that this modifies the surface contact angle according to the expression

$$\cos \theta^* = r \cos \theta \tag{1}$$

where θ^* is the apparent contact angle on the textured surface, r is the surface roughness defined as the actual area divided by the projected area, and θ is the equilibrium contact angle on a smooth surface of the same material, given by Young's equation (29) as $\cos \theta = (\gamma_{sv} - \gamma_{sl})/\gamma_{lv}$, where γ is the interfacial tension and the subscripts s, l, and v refer to the solid, liquid, and vapor phases, respectively.

The Cassie model, on the other hand, postulates that the superhydrophobic nature of a rough surface is due to microscopic pockets of air trapped below the liquid droplet, leading to a composite interface. In recent literature (16), the Cassie–Baxter model is often described using the apparent contact angle on a rough surface by the following equation:

$$\cos \theta^* = -1 + \varphi_s(1 + \cos \theta) \tag{2}$$

where ϕ_s is the fraction of the solid in contact with the liquid. In contrast to the Wenzel relation, the Cassie relation permits $\theta^* > 90°$, even when $\theta < 90°$. Equation 2 is only valid when the liquid is in contact with a flat, porous substrate, i.e., when the top of a rough surface is flat. The original full Cassie–Baxter model (28) is generally written as

$$\cos \theta^* = f_1 \cos \theta - f_2 \tag{3}$$

where f_1 is the surface area of the liquid in contact with the solid divided by the projected area and f_2 is the surface area of the liquid in contact with air trapped in the pores of the rough surface divided by the projected area. According to Cassie and Baxter

$$f_1 = \frac{\text{area in contact with liquid}}{\text{projected area}}$$

$$f_2 = \frac{\text{area in contact with air}}{\text{projected area}} \tag{4}$$

When there is no trapped air, f_1 is identical with the value of r in the Wenzel model. Recognizing this, eq 3 has recently been rewritten as follows (19):

$$f_1 = r_f f \tag{5}$$

$$f_2 = 1 - f \tag{6}$$

$$\cos \theta^* = r_f f \cos \theta + f - 1 \tag{7}$$

where f is the fraction of the projected area of the solid surface in contact with the liquid and r_f is the roughness of the portion of the solid that is in contact with water. When $f = 1$, $r_f = r$ in the Wenzel model. It is important to note that r_f in eq 7 is not the roughness ratio of the total surface but only that in contact with the liquid. In this form of the Cassie–Baxter equation, the contributions of surface roughness and of trapped air are clearer than those in the other forms of the equation.

Thermodynamic considerations can be used to determine whether a particular textured surface will exist in the Wenzel or Cassie state (19, 30). The situation is complicated because of the presence of multiple local free-energy minima, leading to so-called "metastable" configurations (19, 30–33). Careful experimentation with model microstructured surfaces and corresponding free-energy calculations show that a series of rough substrates with progressively increasing equilibrium contact angles exhibit a transition from the Wenzel state to the Cassie state (8, 30, 32, 34). A threshold value of the equilibrium contact angle (θ_c) for this transition is obtained by equating eqs 1 and 2:

$$\cos \theta_c = \frac{\varphi_s - 1}{r - \varphi_s} \tag{8}$$

Because $r > 1 > \phi_s$, the critical value of the equilibrium contact angle θ_c for this transition is necessarily greater than 90°. Thus, it may be anticipated from eq 8 that, for $\theta < 90°$, a surface cannot exist in the Cassie state or that the creation of highly nonwetting surfaces ($\theta^* \gg 90°$) requires $\theta > \theta_c > 90°$. These arguments emphasize the difficulty of developing surfaces for which $\theta^* > 150°$ in contact with alkanes such as decane or octane because there are very few reports of a natural or artificial surface with a sufficiently low surface energy to give $\theta > 90°$ with these liquids. When eqs 1 and 7 are equated, an equilibrium contact angle (θ_c) for this transition is obtained by the following:

$$\cos \theta_c = \frac{-f_2}{r - r_f(1 - f_2)} \tag{9}$$

In contradiction to eq 8, under certain conditions with $r_f > r > f_2$, the critical value of θ_c for this transition is <90°. Equation 8 thus indicates that, for $\theta < 90°$, a surface can exist in a thermodynamically favorable metastable Cassie state or that the creation of highly nonwetting surfaces ($\theta^* \gg 90°$) can be obtained with $\theta < 90°$.

Artificial superhydrophobic surfaces have been fabricated with a variety of organic and inorganic substrates, e.g., polymers (12, 20, 21, 35–37), silicon wafers (17, 18, 38),

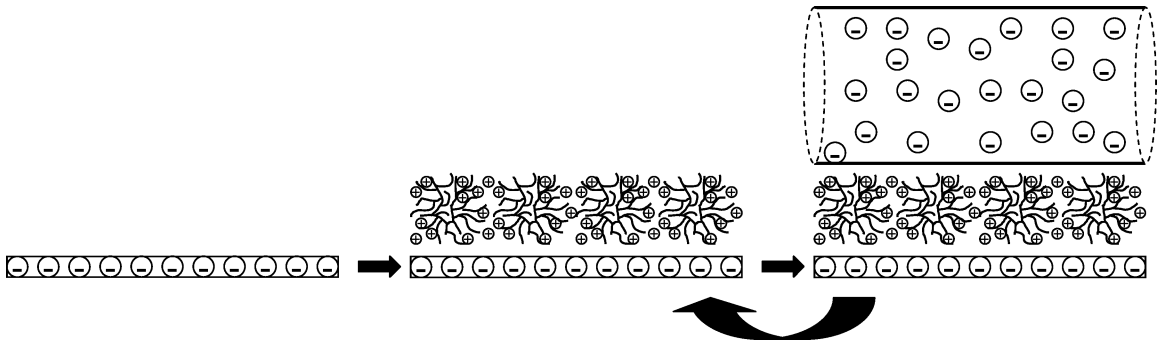

FIGURE 1. Schematic representation of the buildup of electrostatically adsorbed multilayered films. The polyelectrolyte, PEI, is shown as highly branched molecules, and colloidal cellulose nanocrystals are represented by a straight rod; counterions have been omitted for clarity.

glass slides (9, 20) and metals (39). Recent investigations have demonstrated that it is possible to induce superhydrophobic phenomena on intrinsically hydrophilic materials if the surface consists of a microtexture with overhang structures (17, 38, 40). A question of significant interest is whether this principle can be applied to make super-oil-repellent surfaces on intrinsically oleophilic materials because this would greatly expand the range of materials that can be used to manufacture the super-oil-repellent surfaces.

With increasing environmental interest in the use of renewable resources and biodegradable materials, the inorganic substrates listed above are less than ideal. Moreover, they are not mechanically flexible, which limits their processability and therefore the range of potential applications. Organic polymer substrates, on the other hand, are flexible, but they tend to be fairly expensive and often lack biodegradability and renewability. Hence, the search for alternative substrates for highly hydrophobic and oleophobic surfaces is ongoing. Cellulose, a biodegradable, renewable, inexpensive, biopolymer, which is abundantly present in nature, has been suggested as a candidate. If cellulose-based substrates can be rendered superoleophobic by simple processing schemes, they will offer a promising alternative to conventional superoleophobic substrates. Because of their relatively low cost and mechanical flexibility, these surface-modified materials could have applications in a vast array of products, including fast food and microwavable food packages, beverage containers, self-cleaning cartons, labels, paper boards, microfluidic devices, and membranes with low degrees of surface fouling. In this study, we work with a stable aqueous colloidal suspension of cellulose in the native "cellulose I" crystal form, continuing the studies on model cellulose surfaces developed in our laboratory (41−43). The nanocrystals in suspension are stabilized by negative surface charges (carboxyl or sulfate ester groups), which result from the hydrolysis process and give them certain polyelectrolyte properties (44). Electrostatic layer-by-layer (LbL) self-assembled films have been exploited for the fabrication of sophisticated nanocomposite materials (45). In the present study, the hierarchical porous structured silicon substrates are exposed to a solution of oppositely charged polyelectrolyte, poly(ethyleneimine) (PEI), followed by rinsing. The polymeric material adhering to the surface has more than the stoichiometric number of charges required for charge neutralization, and the surface charge is thus reversed. This promotes adsorption of the next oppositely charged polyelectrolyte, the cellulose nanocrystals, and the surface charge is again reversed. The amount of adsorbed polyelectrolyte/cellulose is self-limiting as a result of rinsing, and this allows stepwise film growth.

In this study, we show that nanocrystalline cellulose is amenable to sequential film growth by LbL assembly on structured and flat silicon surfaces, as presented schematically in Figure 1. The hierarchical porous cellulose structure forms textures with overhanging structures on the surface, which induce superoleophobic properties on the intrinsically oleophilic silicon surface. After the cellulose surface has been coated with fluorinated trichlorosilanes, the porous cellulose films are highly oil-repellent to, e.g., castor oil, with θ_{rough} of ca. 150° and a contact-angle hysteresis of 7°, although the coated cellulose surface is intrinsically oleophilic, with θ_{flat} for this oil of less than 90°. The surfaces were thoroughly characterized using contact- and roll-off-angle measurements, X-ray photoelectron spectroscopy (XPS), and field-emission scanning electron microscopy (FE-SEM), and these results are used to link the microstructure of the films to the nonwetting properties of the surfaces. Reports of the preparation and characterization of highly oleophobic surfaces ($\theta \gg 90°$) are very rare (16−18), and for cellulose surfaces, they are, to the authors' knowledge, nonexisting.

EXPERIMENTAL SECTION

Preparation of Structured Silicon Surfaces. Polished silicon wafers (boron-doped p-type; MEMC Electronic Materials SpA, Novara, Italy) were thermally oxidized and patterned in an array of circles with a diameter of 1−2 μm and with a peak-to-peak distance of 2−4 μm using standard photolithography followed by anisotropic plasma etching. The plasma etching was performed by the Bosch process in a STS Multiplex inductively coupled plasma etching system (46). The etching and passivation gases were SF_6 and C_4F_8, respectively, and they were switched during the process. The wafers were etched for 40, 30, 20, and 10 min and are referred to as surfaces A−D, respectively.

Preparation of Fluorinated Cellulose and Silicon Substrates. Plasma-etched and nonetched silicon wafers were used as base substrates for the preparation of cellulose and the fluorinated trichlorosilane coatings. The wafers were cleaned by rinsing with a water/ethanol/water sequence. The surfaces were then hydrophilized, and any contamination was removed by a 3 min treatment in a plasma oven (PDC-002; Harrick

Scientific Inc., Pleasantville, NY) operating at 30 W under reduced air pressure.

A colloidal suspension of cellulose nanocrystals was prepared by acid hydrolysis of a dissolving grade pulp by a previously described method (47). The colloidal sol of cellulose nanocrystals, stabilized by the presence of surface sulfate groups with sodium counterions and washed with deionized water, was used to prepare cellulose I surfaces using a modified procedure based on the method of Edgar and Gray (48).

Model films of nanocrystals were prepared by alternating deposition of poly(ethyleneimine) (PEI; 1 g/L, $M_w = 60\,000$ g/mol, 50% aqueous solution, Acros Organics, USA, Morris Plains, NJ) and the nanocrystals (1 g/L) on flat and structured silica surfaces, leading to the formation of polyelectrolyte multilayers (PEMs) (45). Silica wafers were treated with PEI and nanocrystals up to five bilayers in Milli-Q water to ensure sufficient surface coverage of the nanocrystals. The cellulose and silica samples were immersed in the coating solution, made by dissolving 1 mM (tridecafluoro-1,1,2,2,-tetrahydrooctyl-)trichlorosilane (n-$C_6F_{13}CH_2CH_2SiCl_3$, 97%, Sigma-Aldrich, Madison, WI) in heptane (>99.5%, anhydrous, Sigma-Aldrich). After about 15 min of immersion in this solution, the samples were thoroughly rinsed with heptane and Milli-Q water.

Contact-Angle Measurements. A CAM 200 (KSV Instruments Ltd., Helsinki, Finland) contact-angle goniometer was used for advancing and receding contact- and roll-off-angle measurements. Measurements were performed at room temperature with three probe liquids: castor oil (99.5%, Fluka), hexadecane (>99%, anhydrous, Sigma-Aldrich), and decane (>99%, Sigma-Aldrich). The advancing contact angle was measured by advancing the probe liquid onto the surface using a syringe. The receding angle was measured by slowly removing the probe liquid from a drop already on the surface. The software delivered by the instrument manufacturer calculates the contact angles based on a numerical solution of the full Young−Laplace equation. The contact and roll-off angles were determined at three different positions on each sample. The contact-angle values reported were taken after the contact angle had reached a stable value, typically less than 10 s after deposition of the droplet. Typical errors in the experiments were ±2°. The roll-off angles were measured by placing the surfaces on a level platform and tilting the surface until the drop rolled off. The droplet size was 20 μL. Typical errors in the roll-off experiments were ±2°.

XPS. The XPS spectra were collected with a Kratos Axis Ultra DLD electron spectrometer (Manchester, U.K.) using a monochromated Al Kα source operated at 150 W, with a pass energy of 160 eV for wide spectra and a pass energy of 20 eV for individual photoelectron lines. The surface potential was stabilized by the spectrometer charge neutralization system. Photoelectrons were collected at a takeoff angle of 90° relative to the sample surface, and the depth of analysis was ca. 10 nm. The binding energy scale was referenced to the C 1s line of aliphatic carbon, set at 285.0 eV. The spectra were processed with Kratos software and the CasaXPS program package including experimental values for the atomic sensitivity factors, and peak intensities were determined by integrating the areas under the peaks.

FE-SEM. For microstructural analysis, the specimens were studied with a Hitachi s-4300 field-emission scanning electron microscope to obtain secondary electron images. The specimens were fixed on a metal stub with carbon paint and coated with a 3-nm-thick gold layer using an Agar HR sputter coater.

RESULTS

Figure 2 shows representative top (left column) and tilted (20°) (middle and right columns) SEM micrographs at different magnifications of the nonmodified porous silicon surfaces after the plasma-etching processes. As illustrated in Figure 2a, a substrate with nanosized vertically aligned pillars was formed, separated by large cavities with diameters of ca. 4 μm (referred to as surface A). The top pillar width was estimated to be less than 500 nm, whereas the bottom of the pillar was estimated to be approximately 2 μm. Figure 2b shows SEM micrographs of a surface with a network of irregular domains of nanowires located above a pattern of vertically aligned pillars (surface B). The silicon nanowires were several micrometers long with a width of approximately 200 nm. The silicon nanowires were grown somewhat vertically, pointing outward from the surface. Star-shaped structured pillars were also created, and these are shown in Figure 2c (surface C). The distance between the peaks, i.e., the cavities, is approximately 2 μm. The top surface of the pillars was "star-shaped" with a diameter of approximately 400 nm. Cavities with a width of 4 μm are also seen in Figure 2d (surface D). The surface texture is roughly the same as that in Figure 2c, except for the vertically aligned pillars.

In general, to promote the trichlorosilane coating of the silicon substrates, an activation in oxygen plasma to generate reactive OH groups on the surface was required (18, 49). These activated surfaces can react with functionalized silanes (usually trichlorosilane) in a gaseous or solvent phase to yield spontaneously assembled, often highly organized monolayers with the desired functionality. Trifunctional organosilanes ($RSiX_3$), compared to their monofunctional analogues, are more reactive and are capable of polymerizing in the presence of water, including from ambient humidity, which gives rise to a number of possible thin film structures. Along with the monolayer formation, other covalent attachments and three-dimensional, surface-induced polycondensation are possible (50).

In the work, this coating process is applied to the structured silicon/cellulose surfaces. The unique structure of the coating was found to significantly decrease the wetting properties, as evaluated from contact-angle measurements using three nonpolar liquids: castor oil, hexadecane, and decane with surface tensions of 35.8, 27.5, and 23.8 mN/m, respectively. Table 1 summarizes the advancing contact-angle values at equilibrium (θ_{adv}) and the test liquids on the silicon surfaces modified by plasma treatment and subsequent coating with 1*H*,1*H*,2*H*,2*H*-perfluorooctyltrichlorosilane (PFOTS). As a reference, contact-angle values of PFOTS monolayers on flat surfaces are given.

Plasma treatment of the surface results in complete wettability of the surface for castor oil, hexadecane, and decane. When PFOTS is applied in the refunctionalization step, the structured coatings become nonwettable for all liquids. In general, the structured PFOTS-treated silicon surfaces displayed clear oleophobic properties ($\theta \gg 90°$). The most oleophobic surface, surface A, exhibited advancing contact angles of roughly 169, 144°, and 131° for castor oil, hexadecane, and decane, respectively, which, to the authors' knowledge, are among the highest contact angles found in the literature for these liquids or liquids with similar

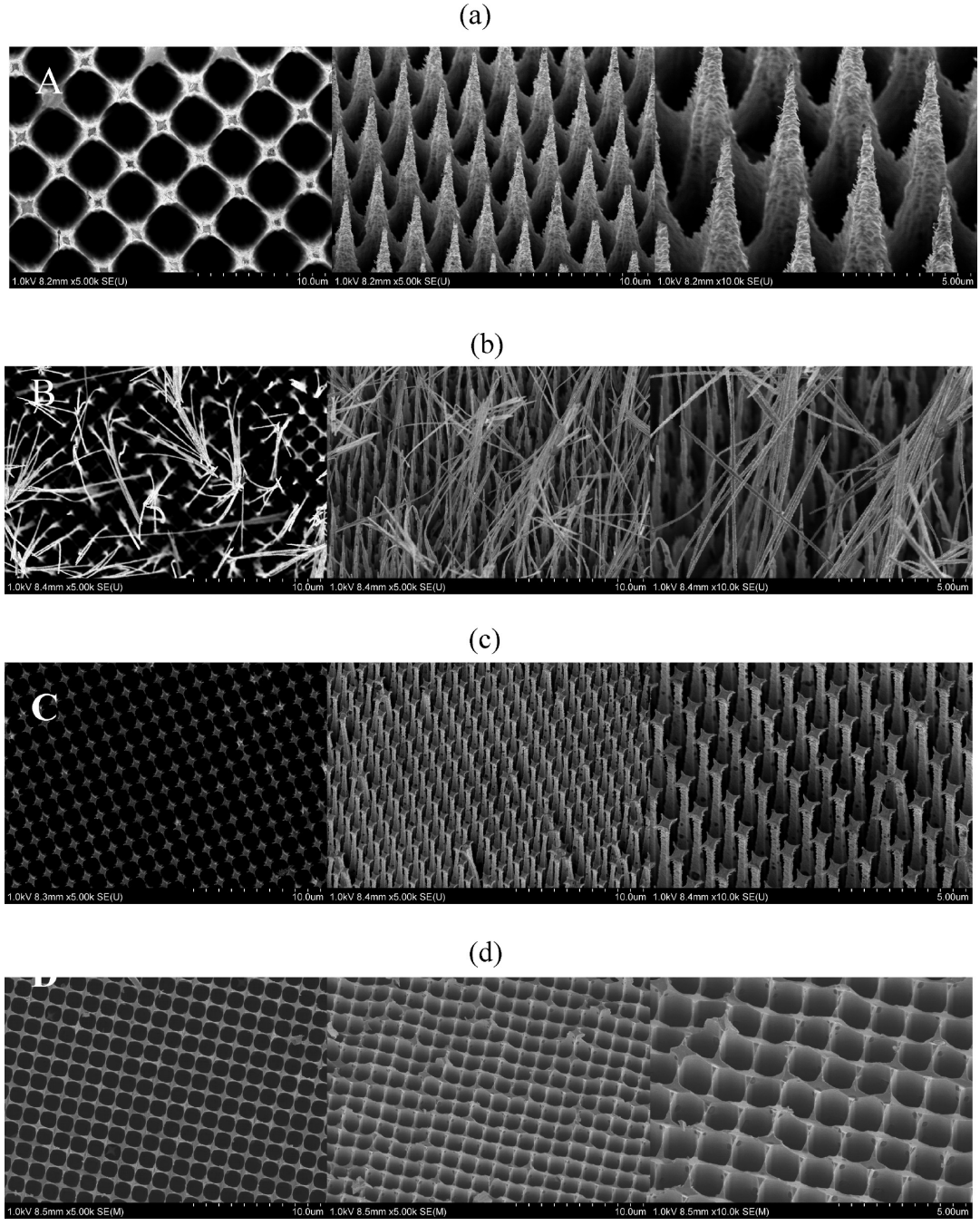

FIGURE 2. SEM micrographs of porous silicon surfaces fabricated by plasma etching. The surfaces are referred to as A−D (from the top). The left-hand column shows the top-view image (magnification 5000×); the middle and right-hand columns show images obtained at a 20° tilt angle at magnifications of 5000× and 10 000×, respectively.

Table 1. Advancing Contact Angles (deg) for Nonpolar Liquids for PFOTS-Coated and Noncoated Structured and Planar Silicon Surfaces

	planar surfaces	planar PFOTS-modified	PFOTS-modified surface A	PFOTS-modified surface B	PFOTS-modified surface C	PFOTS-modified surface D
$\theta_{\text{castor oil}}$	<5	82	167	158	152	142
$\theta_{\text{hexadecane}}$	∼0	68	144	128	120	109
θ_{decane}	∼0	58	131	106	98	81

surface tensions (6, 16−18). As expected, there is a large difference between the contact-angle values on the structured surfaces and those on the planar surfaces.

To judge whether the structured silicon surfaces were truly superoleophobic, the contact-angle hysteresis and roll-off angles were measured. For surface A, castor oil, hexadecane, and decane roll-off angles were determined to be 10, 12, and 13°, respectively. For comparison, the roll-off angle for water was as low as <5°. For surfaces B−D, the roll-off angles were determined to be ca. 15−25° for the different probe liquids. The roll-off angles were found to be highly dependent on the volume of the droplets. For instance, for surface A, the roll-off angle ranged from 20° for a 10 μL droplet to 10° for a 20 μL droplet. For surface A, contact-angle hysteresis values of 2, 2, and 1° were found

Table 2. Atomic Surface Concentrations on PFOTS-Coated and Noncoated Structured and Planar Silicon Surfaces

	surface concentration (atom %)			
	C	O	Si	F
pure silicon surfaces	7	39	54	
planar PFOTS-coated silicon surface	26	13	20	41
structured PFOTS-coated silicon surfaces	25	17	15	43

for castor oil, hexadecane, and decane, respectively. For surfaces B−D, the contact-angle hysteresis was determined to be <10° for the different probe liquids.

The surface compositions of the planar and structured reference surfaces and their fluorinated analogues are given in Table 2. Survey spectra (data not shown) of the pure silicon surfaces showed the presence of only silicon and oxygen (and small amounts of carbon) on the surface. Hydrocarbons tend to be the most common surface contamination, and it is quite common to observe traces of contaminants giving rise to C 1s spectra of silicon surfaces. The surface composition was significantly changed when PFOTS was adsorbed onto the surfaces, as shown in Table 2. The total oxygen concentration decreased from 39% to 13%, and the fluorine concentration was found to be 41%. The atomic surface concentrations of carbon, oxygen, silicon, and fluorine was very similar for all of the structured PFOTS-coated surfaces. As in the case of the planar fluorinated silicon surfaces, the fluorine signal from the structured silicon surfaces was determined to be >40%, indicating reproducible results from the PFOTS coating. The error of the XPS determinations was within ±2%.

Parts a and b of Figure 3 are SEM micrographs of a planar cellulose film at two magnifications, 40 000× and 60 000×, respectively, and it is evident that the cellulose nanocrystals were successfully incorporated into PEM films containing PEI and adsorbed onto the planar silicon surfaces. The random orientation and distribution of the nanocrystals is apparent in the micrographs. The micrograph also indicates some porosity. Cellulose nanocrystals were estimated to have dimensions of ca. 10 nm × 200 nm. The length polydispersity of the nanocrystals is apparent and has also been previously found to be 1.2−1.3 (51, 52). Figure 4 gives SEM micrographs of silicon surface C (Figure 4a,c) and its cellulose-modified analogue (Figure 4b,d) at two magnifications, 2000× and 10 000×, respectively. The SEM micrographs indicate that the structured silicon surfaces are covered with cellulose and that the coated silicon pillars/wires are rougher and broader than the uncoated ones. This was, in particular, observed at a magnification of 10 000×, where a filmlike structure is apparent on the nanowires (Figure 4c,d).

The wetting properties of the cellulose surfaces were evaluated using castor oil, hexadecane, and decane (Table 3). In general, the PFOTS-treated cellulose surfaces displayed highly oleophobic properties. The wetting properties of the surfaces are clearly influenced by the topography. Before PFOTS coating, the cellulose surfaces are oleophilic with advancing contact angles for castor oil, hexadecane, and decane of less than 5°. After PFOTS coating of the flat cellulose surface, the θ_{adv} values for castor oil, hexadecane, and decane on PFOTS-coated cellulose were 72, 60, and 48°, respectively. When a coating was applied to structured cellulose films, they displayed highly oleophobic properties with an advancing contact angle in the vicinity of 140° for castor oil. This is interesting considering the fact that the PFOTS-coated planar cellulose is intrinsically oleophilic (θ_{adv} < 90° for all oils). The roll-off angles for castor oil, hexadecane, and decane on the PFOTS-coated cellulose surface A were 13, 15, and 16°, respectively. For the cellulose-modified surfaces B−D, the roll-off angles were determined to be ca. 20−30° for the different probe liquids. Again, the roll-off angles were found to be highly dependent on the volume of the droplets. For the PFOTS-coated cellulose surface A, contact-angle hysteresis values of 4, 4, and 2° were found for castor oil, hexadecane, and decane, respectively. For the PFOTS-coated cellulose surface B−D, the contact-angle hysteresis values were determined to be <10° for the different probe liquids.

XPS measurements strongly support that a successful chemical modification of the cellulose surfaces has been achieved. A summary of the atomic concentrations for pure and PFOTS-coated planar and structured cellulose is given in Table 4. Survey spectra of the cellulose films showed carbon, oxygen, and small amounts of nitrogen and sulfur on the surface. The trace amounts of sulfur are due to sulfate ester groups resulting from hydrolysis with sulfuric acid during preparation of the cellulose nanocrystals. Taking into account the fact that the depth of analysis by XPS is about 10 nm, this indicates a dense film characteristic with a thickness of >10 nm and that a complete surface coverage of the silicon substrate occurred after 10 adsorption steps (five bilayers) with the solution-dipped films. The films show higher carbon and lower oxygen contents than expected from the chemical composition of anhydroglucose $(C_6O_5H_9)_n$, probably because of PEI incorporated with the cellulose nanocrystal network. As in the case of the PFOTS-coated cellulose surfaces, the amount of fluorine at the surface increased, while the amounts of carbon, oxygen, nitrogen, and sulfur decreased. The amount of fluorine on the cellulose surface after coating (ca. 31−34%) was found to be slightly lower than that on the fluorinated silicon surfaces (ca. 41−43%).

DISCUSSION

The wettability of a cellulose surface is important because it controls the interaction of the surfaces with liquids and other solid surfaces and, hence, dominates in the properties of most cellulose-based products. The wetting is governed by both the chemical composition and the geometrical structure of the surface.

In the present study, the surface chemistry has been controlled by the presence of fluoroallylsilane groups covalently bonded to the hydroxylic groups of the silicon and cellulose surfaces. The atomic fluorine and carbon concentrations of pure fluorinated trichlorosilane were determined

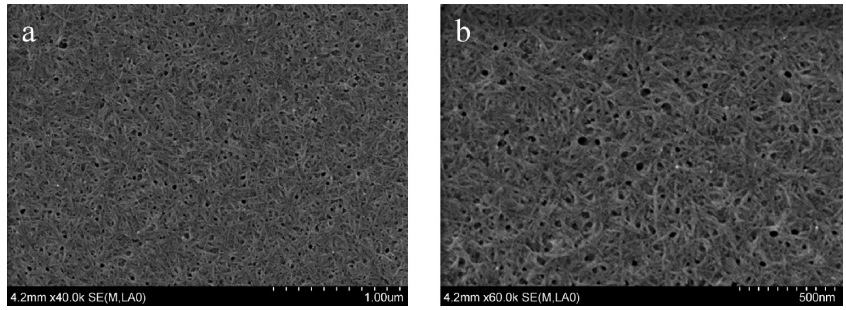

FIGURE 3. SEM micrographs at magnifications of (a) 40 000× and (b) 60 000× of multilayered films of PEI and cellulose nanocrystals (five bilayers) prepared by solution dipping of a planar silicon surface.

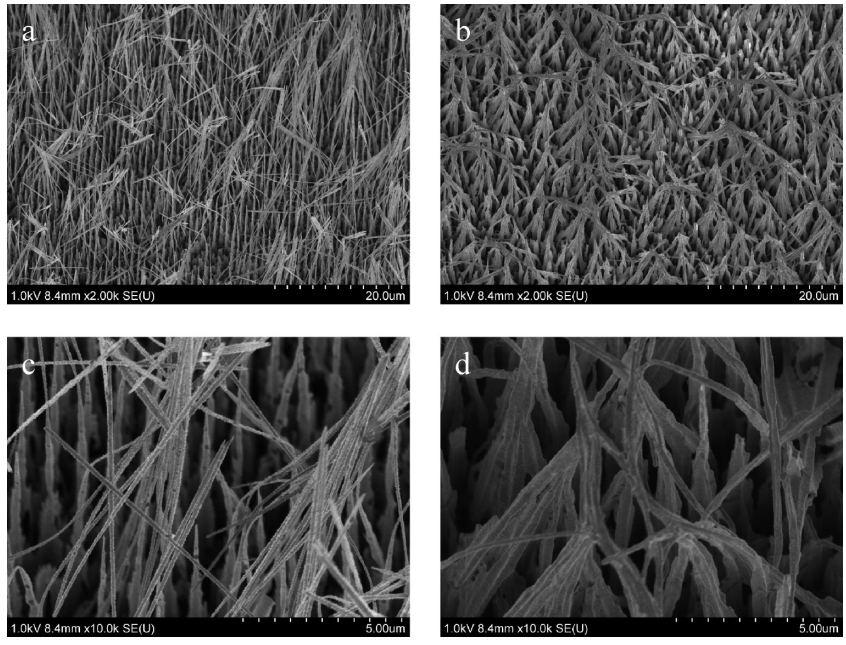

FIGURE 4. SEM micrographs of silicon surface C (a and c) multilayered with PEI and cellulose nanocrystals (five bilayers) (b and d) at magnifications of 2000× (a and b) and 100 000× (c and d).

Table 3. Advancing Contact Angles (deg) for Nonpolar Liquids on PFOTS-Coated and Noncoated Structured and Planar Cellulose Nanocrystal Surfaces

	planar cellulose surfaces	planar PFOTS-modified cellulose	PFOTS-modified cellulose surface A	PFOTS-modified cellulose surface B	PFOTS-modified cellulose surface C	PFOTS-modified cellulose surface D
$\theta_{\text{castor oil}}$	<5	72	146	141	133	125
$\theta_{\text{hexadecane}}$	~0	60	128	113	105	108
θ_{decane}	~0	48	107	98	79	88

by XPS to be approximately 53 and 37%, respectively. Because the depth of XPS analysis is on the order of 10 nm and significant amounts of silicon (ca. 15−20%) and carbon (ca. 45%) were detected by XPS for the PFOTS-coated silicon and cellulose surfaces, respectively, it is believed that the fluorinated trichlorosilane is adsorbed in the form of very thin films (<10 nm).

The high concentrations of $-CF_2$ and $-CF_3$ groups, together with the relatively high ratio of $-CF_3$ to $-CF_2$ groups (spectrum not shown), as indicated by XPS analysis, result in very oleophobic materials with low surface energy. The dispersive surface energy of the flat silicon and cellulose surfaces was determined by contact-angle measurements, using hexadecane as the probe liquid and the following version of Young's equation (53, 54):

$$2\sqrt{\gamma_s^d \gamma_l^d} = \gamma_l(1 + \cos\theta_e) \qquad (10)$$

where γ_s^d is the dispersive surface energy of the silicon/cellulose surface, γ_l^d the dispersive surface tension of the liquid, γ_l the surface tension of the liquid, and θ_e the equilibrium contact angle between the liquid and the silicon/

Table 4. Atomic Surface Concentrations on PFOTS-Coated and Noncoated Structured and Planar Cellulose Surfaces

	surface concentration (atom %)					
	C	O	N	S	Si	F
cellulose nanocrystal surfaces	60	38	2	1		
planar PFOTS-coated cellulose surfaces	46	20	1		2	31
structured PFOTS-coated cellulose surfaces	45	18	1		2	34

cellulose surface. This equation is valid when the interactions between the liquid and the surface are dominated by dispersive interactions. The values determined for the flat silicon and cellulose surfaces were 13 and 15 mN/m, respectively.

Among the numerous molecular structures investigated, a close-packed uniform CF_3 surface has been found to possess the lowest surface free energy measured (ca. 6.7 mN/m) (25). The critical surface tension for CF_2-CF_2 groups was determined by Zisman et al. to be 18 mN/m (55), which indicates that the PFOTS-coated surfaces are strongly enriched by CF_3 groups. Taking this into consideration, these studies can explain why the flat silicon and cellulose surfaces displayed contact angles for hexadecane and decane of less than 90° because these surfaces would need surface energies of ca. 6.9 and 6.0 mN/m, respectively, to display $\theta >$ 90° with these liquids.

Because the surface composition is almost the same for the PFOTS-coated planar and structured celluloses, the structure-induced roughness should be taken as the primary cause of the large difference in the oleophobicity of these surfaces. The increase in the oleophobicity due to a rough or microstructured surface can be interpreted in terms of models originally described by Wenzel (27) and by Cassie and Baxter (28). In the Wenzel model, the liquid is in contact with the entire solid surface and completely penetrates the gaps generated by the roughness. The effect of the surface roughness in this model is simply to increase the surface area. Therefore, the enhanced oleophobicity in this study is believed to be a purely geometric effect. In contrast, the Cassie–Baxter model assumes that the liquid rests on the rough features of the protruding solid material. The air entrapped by these features then acts as a further support for oil droplets, so that the apparent contact angle of the oil on the substrate is a composite effect of the interaction between the oil droplet and the solid and the oil droplet and air.

The key feature of the structured surfaces in this study is that they possess the desired characteristics of both "roughness" (i.e., $r > 1$) and a low value for the wetted surface fraction (i.e., $\phi_s < 1$, $f_2 \gg f_1$) embodied in eqs 1–3. As a consequence of the multiple scales of roughness and high porosity generated by the plasma-etching process, the samples are expected to be best characterized by the Cassie equation.

An important observation in Tables 1 and 3 is that the advancing contact angles for the PFOTS-coated structured surfaces are >90°, even though in each case the advancing contact angles for the smooth surfaces are <90°. This is surprising if it is assumed that for $\theta < 90°$ the rough surfaces are in the Wenzel state, and from eq 1, $\theta^* < \theta$ is expected. This unusual effect is further shown in the general wetting diagram (16) in Figure 5a, which shows a plot of cos θ^* on the rough PFOTS-coated silicon surfaces as a function of cos θ for the corresponding PFOTS-coated smooth surfaces. The surfaces display high apparent advancing contact angles (θ^*), suggesting that they are best described by the Cassie–Baxter

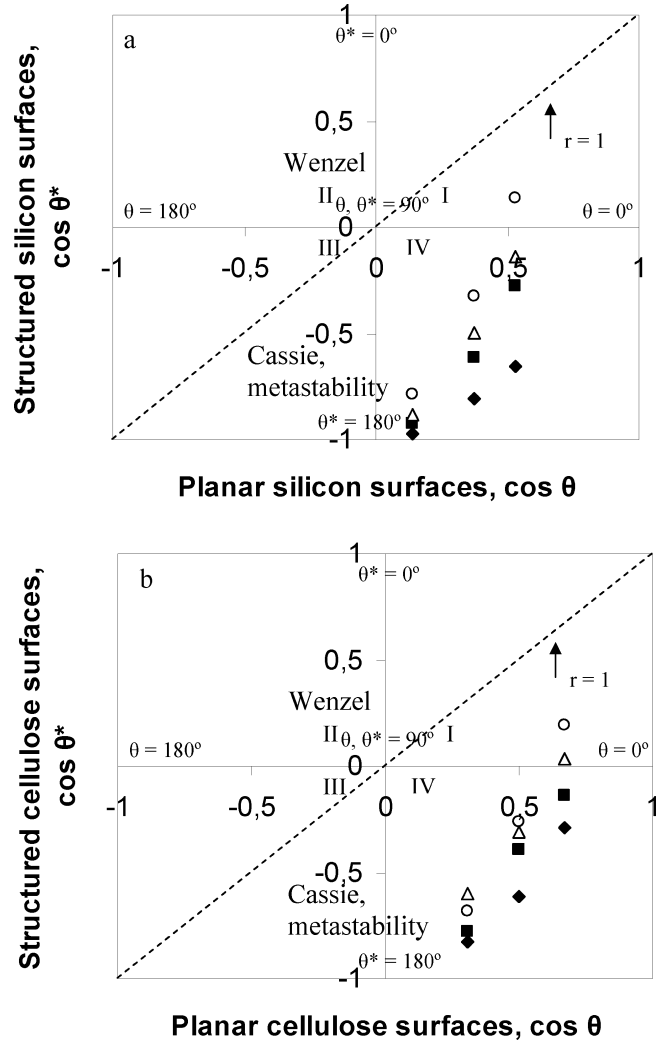

FIGURE 5. Nonwetting diagrams comparing the contact angles for various alkanes: castor oil, hexadecane, and decane (left to right), on the structured and planar PFOTS-coated silicon (a) and cellulose (b) surfaces. Surfaces A–D are ◆, ■, Δ, and ○, respectively. The multiple scale of roughness generated by the plasma-etching process promotes the formation of a composite interface (the Cassie state) even with $\theta < 90°$. The surfaces in the lower right quadrant of these diagrams correspond to oleophilic substrates that are rendered oleophobic purely by topography.

equation. Earlier experiments show that this Cassie state is metastable, i.e., only locally stable, and that the energy barrier separating the Cassie and Wenzel states is dependent on the topography of the surfaces under consideration (7, 8, 32). It has also been suggested that this energy barrier may be provided by a capillary force that prevents liquid from entering into the indentations present at the surface (38). However, it is clear in Figure 5a that a transition from the Wenzel state to the nonwetting Cassie state can be observed at an equilibrium contact angle, θ_c, of less than 90°.

The PFOTS-coated structured cellulose surfaces also display highly oleophobic properties ($\theta^*_{adv} \gg 90°$), even though all of the corresponding PFOTS-coated cellulose surfaces are oleophilic ($\theta_{adv} < 90°$). Table 3 shows that, in most cases, θ^* values for castor oil, hexadecane, and decane on the rough cellulose surfaces are much greater than 90°. Thus, a

possible transition from the Wenzel state to the metastable Cassie state can be observed for each alkane (Figure 5b). This metastable state has previously been found to be related to a local minimum in free energy that systematically shifts to lower surface energy with decreasing liquid surface tension (16).

Nevertheless, the design of metastable highly oleophobic ($\theta^* \gg 90°$) silicon and cellulose surfaces even with the limitation to materials with $\theta < 90°$ can be modeled solely with the reformed Cassie–Baxter equation (19, 56). According to eq 9, under certain conditions, the wetting equilibrium can, when $r_f > r > f_2$ and $\theta < 90°$, exist in a mathematically thermodynamically favorable Cassie state. Thus, this is in some perspective in contradiction to a possible transition from the Wenzel state to the metastable Cassie state. As was recently realized, the role of a possible transition between the wetting states of highly oleophobic materials is not yet clear (19).

While the advancing contact angle of oils has been commonly used as a criterion for the evaluation of hydrophobicity or oleophobicity, additional information about the wetting properties of surfaces can be obtained from contact-angle hysteresis and roll-off-angle measurements (10, 16, 57). The present results show that the roll-off angles are affected by the surface texture such as the needle size and peak-to-peak distance. In the highly oleophobic systems studied here, i.e., surface A (both pure and cellulose-modified), the roll-off angles decrease for larger advancing contact angles. As was previously discussed, the results suggest that the air trapped in the surface structure plays an important role for a surface with a low roll-off angle and low contact-angle hysteresis. The variable resistance offered to the receding meniscus of the sliding drop was earlier found to be proportional to the total number of reentrant structural elements at the air–liquid–solid three-phase contact line (16). The needlelike structure of surface A shown in Figure 2a may serve as a means of trapping sufficient air for low roll-off angles to be exhibited. Surface structures such as that shown in Figure 2a have projections with proper heights at proper intervals to trap sufficient air in the structure. Surfaces B–D exhibited higher roll-off angles compared with surface A. These results are in agreement with eqs 2 and 3, which suggest that the advancing contact and roll-off angles should increase and decrease, respectively, with decreased wetted area fraction (ϕ_s, f_1). However, it should be stressed that a surface with a high contact angle does not always show a low roll-off angle. In particular, the mechanism of roll-off is not yet fully understood. For example, Murase et al. demonstrated that a fluoropolymer with a water contact angle of 117° shows a higher roll-off angle than a poly(dimethylsiloxane) with a water contact angle of 102° (58).

The contact-angle hysteresis is believed to be governed by several factors, i.e., surface roughness, chemical heterogeneity, and surface structure. A hysteresis effect between the advancing and receding contact angles can also be viewed as an indication of the extent of the change in the surface properties caused by the wetting. The PFOTS-coated surfaces studied in this work exhibit low hysteresis for all probe liquids used. The results indicate chemically homogeneous surfaces and very low, if any, liquid intrusion into the cavities of these surfaces. This is expected because the highly fluorinated species, i.e., $-CF_3$ and $-CF_2$ groups, have very low surface free energy, resulting in low intermolecular interactions with, for example, liquids and oils. The fluorinated silanes are covalently attached to the cellulose and silicon surfaces, respectively, and are therefore less prone to reorientation. The contact-angle hysteresis may reflect the properties not only of the solid but also of the liquids. Indeed, Lam et al. (59) found that, for fluorinated silicon surfaces, the hysteresis increased systematically using alkanes with gradually lower surface tensions. However, from the present results, it is difficult to draw such conclusions.

In this study, we have shown the existence of the metastable Cassie state on silicon and cellulose surfaces with well-defined topography and a θ_{flat} of less than 90° and that the wetting interface and the stability/robustness of this state is governed by the overhanging structures. Tuteja et al. (16) stated that the stability/robustness of the metastable state is governed by two important design parameters: a spacing ratio, D, and a robustness parameter, H. The spacing ratio (D) is defined by the edge-to-edge spacing of, for example, nanofibers, nanopillars, and nanowires, and H, which measures the robustness of the metastable Cassie state with respect to the fluid properties, equilibrium contact angle, and surface geometry, is determined by measuring the height of the liquid required to force the liquid through a fiber network/film. However, it is clear that to maximize both θ^* and the stability of the Cassie state, sparsely spaced, highly reentrant surfaces with both $H^* \gg 1$ and $D^* \gg 1$ are desirable.

Tsuji et al. (60) discuss the transition from the Wenzel state to the metastable Cassie state and presume that the unusual wetting behavior is due to a different arrangement of fluoroalkyl groups on the rough and flat silicon substrates. The same may possibly apply to the present study in the case of the modified cellulose, but further studies must be performed to ascertain whether there is a possible contradiction in the Wenzel equation in these cases or whether the observations are only an artifact due to different arrangements of fluoroalkyl groups on the surfaces. Angular-dependent XPS may provide information about the uniformity and orientation of the fluoroalkyl groups on the surfaces (61).

The relation between the advancing contact angles and the surface energy should be expected to depend on the concentration of fluorine on the silicon and cellulose surfaces. XPS measurements indicate that the concentration of fluorine is slightly higher after PFOTS coating on the silicon surfaces than on the corresponding cellulose surfaces. It is difficult to draw any conclusions, but the results indicate more exposed and reactive –COH groups in silica than in the cellulose nanocrystals. The high crystalline ordering of the nanocrystals (62), and, thus, the presumably less available –OH groups for molecular bonding, naturally affects their interaction with other materials and liquids. Further,

the plasma-induced activation of the silicon surfaces may result in more reactive −OH groups compared with the nanocrystals.

CONCLUSIONS

We have demonstrated a plasma-etching approach for making hierarchical structured silicon surfaces that are able, after PFOTS coating, to induce a superoleophobic phenomenon on intrinsically oleophilic silicon surfaces. The porous structure of the surfaces forms overhang structures, and these play, including the surface free energy of the surfaces, an important role in inducing the superoleophobic phenomena. Silicon surfaces were also coated with cellulose nanocrystals using the PEM technique. After coating of the cellulose surface with PFOTS, the porous cellulose films displayed highly nonwetting properties for a number of liquids with low surface tension, including alkanes such as hexadecane and decane. It is anticipated that this approach and principle could be applied to expand the range of materials that can be used to fabricate superoleophobic cellulose surfaces. Further efforts could concentrate on the application of highly oleophobic cellulose surfaces to textiles, coatings, packaging, microfluid channels, and nonwetting liquid-transfer and chemical industries.

Acknowledgment. We thank BIM Kemi Sweden AB and the Knowledge Foundation through its graduate school YPK for financial support. We gratefully acknowledge Professor Lars Ödberg for valuable discussions.

REFERENCES AND NOTES

(1) Barthlott, W.; Neinhuis, C. *Planta* **1997**, *202*, 1–8.
(2) Genzer, J.; Efimenko, K. *Biofouling* **2006**, *22*, 339–360.
(3) Parker, A. R.; Lawrence, C. R. *Nature* **2001**, *414*, 33–34.
(4) Gao, X.; Jiang, L. *Nature* **2004**, *432*, 36.
(5) Autumn, K.; Liang, Y. A.; Hsleh, S. T.; Zesch, W.; Chan, W. P.; Kenny, T. W.; Fearilng, R.; Full, R. J. *Nature* **2000**, *405*, 681–686.
(6) Onda, T.; Shibuichi, S.; Satoh, N.; Tsujii, K. *Langmuir* **1996**, *12*, 2125–2127.
(7) Marmur, A. *Langmuir* **2004**, *20*, 3517–3519.
(8) Lafuma, A.; Quere, D. *Nat. Mater.* **2003**, *2*, 457–460.
(9) Yabu, H.; Takebayashi, M.; Tanaka, M.; Shimomura, M. *Langmuir* **2005**, *21*, 3235–3237.
(10) Miwa, M.; Nakajima, A.; Fujishima, A.; Hashimoto, K.; Watanabe, T. *Langmuir* **2000**, *16*, 5754–5760.
(11) Yoshimitsu, Z.; Nakajima, A.; Watanabe, T.; Hashimoto, K. *Langmuir* **2002**, *18*, 5818–5822.
(12) Erbil, H. Y.; Demirel, A. L.; Avci, Y.; Mert, O. *Science* **2003**, *299*, 1377–1380.
(13) Feng, L.; Li, S.; Li, Y.; Li, H.; Zhang, L.; Zhai, J.; Song, Y.; Liu, B.; Jiang, L.; Zhu, D. *Adv. Mater.* **2002**, *14*, 1857–1860.
(14) Feng, L.; Li, S.; Li, Y.; Li, H.; Zhang, L.; Zhai, J.; Song, Y.; Liu, B.; Jiang, L.; Zhu, D. *Adv. Mater. (Weinheim, Germany)* **2002**, *14*, 1857–1860.
(15) Ahuja, A.; Taylor, J. A.; Lifton, V.; Sidorenko, A. A.; Salamon, T. R.; Lobaton, E. J.; Kolodner, P.; Krupenkin, T. N. *Langmuir* **2008**, *24*, 9–14.
(16) Tuteja, A.; Choi, W.; Ma, M.; Mabry, J. M.; Mazzella, S. A.; Rutledge, G. C.; McKinley, G. H.; Cohen, R. E. *Science* **2007**, *318*, 1618–1622.
(17) Cao, L.; Price, T. P.; Weiss, M.; Gao, D. *Langmuir* **2008**, *24*, 1640–1643.
(18) Zimmermann, J.; Rabe, M.; Artus, G. R. J.; Seeger, S. *Soft Matter* **2008**, *4*, 450–452.
(19) Marmur, A. *Langmuir* **2003**, *19*, 8343–8348.
(20) Coulson, S. R.; Woodward, I. S.; Badyal, J. P. S.; Brewer, S. A.; Willis, C. *Chem. Mater.* **2000**, *12*, 2031–2038.
(21) Balu, B.; Breedveld, V.; Hess, D. W. *Langmuir* **2008**, *24*, 4785–4790.
(22) Gao, L.; McCarthy, T. J. *Langmuir* **2007**, *23*, 3762–3765.
(23) Gao, L.; McCarthy, T. J. *Langmuir* **2006**, *22*, 6234–6237.
(24) Gao, L.; McCarthy, T. J. *Langmuir* **2006**, *22*, 2966–2967.
(25) Hare, E. F.; Shafrin, E. G.; Zisman, W. A. *J. Phys. Chem.* **1954**, *58*, 236–239.
(26) Pittman, A. G.; Sharp, D. L.; Ludwig, B. A. *J. Polym. Sci., Part A-1: Polym. Chem.* **1968**, *6*, 1729–1740.
(27) Wenzel, R. N. *J. Ind. Eng. Chem.* **1936**, *28*, 988–994.
(28) Cassie, A. B. D.; Baxter, S. *Trans. Faraday Soc.* **1944**, *40*, 546–551.
(29) Young, T. *Philos. Trans. R. Soc., London* **1805**, 95.
(30) Werner, O.; Wgberg, L.; Lindstroem, T. *Langmuir* **2005**, *21*, 12235–12243.
(31) Patankar, N. A. *Langmuir* **2004**, *20*, 7097–7102.
(32) He, B.; Patankar, N. A.; Lee, J. *Langmuir* **2003**, *19*, 4999–5003.
(33) Patankar, N. A. *Langmuir* **2003**, *19*, 1249–1253.
(34) Barbieri, L.; Wagner, E.; Hoffmann, P. *Langmuir* **2007**, *23*, 1723–1734.
(35) Gao, L.; McCarthy, T. J. *Langmuir* **2006**, *22*, 5998–6000.
(36) Teshima, K.; Sugimura, H.; Inoue, Y.; Takai, O.; Takano, A. *Appl. Surf. Sci.* **2005**, *244*, 619–622.
(37) Youngblood, J. P.; McCarthy, T. J. *Macromolecules* **1999**, *32*, 6800–6806.
(38) Cao, L.; Hu, H.-H.; Gao, D. *Langmuir* **2007**, *23*, 4310–4314.
(39) Qian, B.; Shen, Z. *Langmuir* **2005**, *21*, 9007–9009.
(40) Cao, A.; Cao, L.; Gao, D. *Appl. Phys. Lett.* **2007**, *91*, 034102/1–034102/3.
(41) Aulin, C.; Varga, I.; Claesson, P. M.; Wågberg, L.; Lindström, T. *Langmuir* **2008**, *24*, 2509–2518.
(42) Wågberg, L.; Decher, G.; Norgren, M.; Lindström, T.; Ankerfors, M.; Axnäs, K. *Langmuir* **2008**, *24*, 784–795.
(43) Enarsson, L.-E.; Wagberg, L. *Biomacromolecules* **2009**, *10*, 134–141.
(44) Dong, X. M.; Revol, J.-F.; Gray, D. G. *Cellulose* **1998**, *5*, 19–32.
(45) Decher, G. *Science* **1997**, *277*, 1232–1237.
(46) Bogue, R. *Sens. Rev.* **2002**, *22*, 41–45.
(47) Dong, X. M.; Kimura, T.; Revol, J.-F.; Gray, D. G. *Langmuir* **1996**, *12*, 2076–2082.
(48) Edgar, C. D.; Gray, D. G. *Cellulose* **2003**, *10*, 299–306.
(49) Duffy, D. C.; McDonald, J. C.; Schueller, O. J. A.; Whitesides, G. M. *Anal. Chem.* **1998**, *70*, 4974–4984.
(50) Fadeev, A. Y.; McCarthy, T. J. *Langmuir* **2000**, *16*, 7268–7274.
(51) Cranston, E. D.; Gray, D. G. *Biomacromolecules* **2006**, *7*, 2522–2530.
(52) Marchessault, R. H.; Morehead, F. F.; Koch, M. J. *J. Colloid Sci.* **1961**, *16*, 327–344.
(53) Van Oss, C. J. *Interfacial Forces in Aqueous Media*; Marcel Dekker: New York, 1994.
(54) Van Oss, C. J.; Ju, L.; Chaudhury, M. K.; Good, R. J. *J. Colloid Interface Sci.* **1989**, *128*, 313–319.
(55) Holmberg, K.; Lindman, B.; Joensoon, B.; Kronberg, B. *Surfactants and Polymers in Aqueous Solution*, 2nd ed.; Wiley: London, 2002.
(56) Marmur, A. *Langmuir* **2008**, *24*, 7573–7579.
(57) Michielsen, S.; Lee, H. J. *Langmuir* **2007**, *23*, 6004–6010.
(58) Murase, H.; Nanishi, K.; Kogure, H.; Fujibayashi, T.; Tamura, K.; Haruta, N. *J. Appl. Polym. Sci.* **1994**, *54*, 2051–2062.
(59) Lam, C. N. C.; Kim, N.; Hui, D.; Kwok, D. Y.; Hair, M. L.; Neumann, A. W. *Colloids Surf., A* **2001**, *189*, 265–278.
(60) Tsujii, K.; Yamamoto, T.; Onda, T.; Shibuichi, S. *Angew. Chem.* **1997**, *36*, 1011–1012.
(61) Gerenser, L. J.; Pochan, J. M.; Mason, M. G.; Elman, J. F. *Langmuir* **1985**, *1*, 305–312.
(62) Aulin, C.; Ahola, S.; Josefsson, P.; Nishino, T.; Hirose, Y.; Österberg, M.; Wågberg, L. *Langmuir* **2009**, in press.

AM900394Y